Libyan Journal of Applied and Contemporary Sciences
ISSN
E: 3136-3709
L: 3136-3695
Vol 1: No 2

Optimization of Laser-Induced Optical Response in Advanced Materials for High-Performance Photonic Applications

Fathia Abdelsalam Milad

Department of Mathematical and Physical Studies – Physics Division, Faculty of Science, University of Sirte

Email corresponding author's: fathia.abd@su.edu.ly

Received: 1/7/2026 Accepted: 23/8/2026 Published:28/8/2026

Abstract

Many photonic switches, modulators, sensors and spectral-control devices are based on light-induced variations in the refractive index. It is difficult to find a suitable material, because published nonlinear coefficients depend on wavelength, pulse duration, and measurement method. To address this, we performed a loss-aware analysis on publicly available experimental data. The dataset consisted of 366 nonlinear-index measurements from 240 source records and covered 96 materials. In all cases the linear refractive-index and extinction data were fitted at the same wavelength as the nonlinear measurement. These values were used in a Kerr phase-shifter model that related material response to transmission, interaction length and drive intensity. We tested 5,346 material-band-length combinations. Realizable designs required at least 90% linear transmission, pi-pulse intensity not exceeding 100 GW cm^{-2}, and index change less than 1%. These conditions left 820 designs from 23 material-band pairs, including 75 non-dominated solutions. The optimum trade-off was found for GaAs at 1064 nm, which gives a modeled pi-shift intensity of 3.98 GW cm-2 over 0.410 mm. That estimate, however, came from one nonlinear source. Silicon at 1550 nm was fifth with four sources, with a median nonlinear index of 6.35 $\times 10^{-18}$ m^2 W^{-1}. The clustered meta-regression explained 74.7 % of the observed variance, and the grouped cross-validation yielded a mean R2 of 0.534. Even after correction, measurements of semiconductors remained higher than the chalcogenide reference group. The created shortlist is useful for screening, but direct validation of non-linear absorption, damage limits and waveguide confinement is still needed.

Keyword : nonlinear refractive index; Kerr effect; laser-material interaction; photonic materials; optical switching; Pareto optimization; secondary experimental data; reproducible photonics
Doi : https://doi.org/10.64943/ljacs.2026.010207

INTRODUCTION

Increasingly, modern photonic circuits are using one optical signal to control another, skipping some intermediate electronic conversions. The Kerr effect is attractive in this respect as illumination changes the refractive index of a material. The modulation can be in phase, resonance, polarization, or propagation, depending on the device.

Although the governing material relation is compact, the choice of device material is not. The strong absorption of the material can lead to a large nonlinear coefficient. The expected benefit can be further reduced by two-photon absorption and free carriers. Also the reported values are dependent on pulse duration and crystal orientation so that the coefficient magnitude alone is not a complete selection rule.

With the advent of accurate measurements of the nonlinear refraction, trustworthy comparison became possible. For instance, the single-beam Z-scan can give the sign and magnitude of the response [14]. Further measurements in semiconductors, glasses, crystals and infrared materials have recorded coefficients varying by several orders of magnitude [1, 13].

This trade off is well illustrated by silicon. The Kerr response is good and the fabrication technology is mature. Nonlinear loss is still important in the telecommunications band. Kerr and two-photon coefficients were measured from 850 to 2200 nm by Bristow et al. [3], and Lin et al. [9] resolved clear spectral dispersion. However, short silicon waveguides have been able to provide significant phase control in functional switches [2, 8].

The candidate pool becomes wider in the infrared, where GaAs, Ge, ZnSe, and related crystals are used with mid-infrared lasers. Their nonlinear response can be significant over wide spectral regions although the active absorption processes may vary with pulse duration. Ensley and Bambha [5] studied several infrared materials under ultrafast excitation. Most recently the work of Matteo et al. [10] compared the femtosecond and picosecond behavior near 10.6 μm.

Comparisons available are typically limited to one material family or a narrow laser band. Nonlinear strength and linear loss are also given in separate tables. Hence a large coefficient may appear attractive even when the transmission is poor, and an impressive value obtained in a single experiment may be given undue weight.

RefractiveIndex.INFO collects traceable linear and nonlinear optical constants that allow a wider comparison. Its non-linear entries preserve wavelength, measurement conditions, machine-readable units and links to the original references [12].

We used this tool to screen for materials with linear loss in mind. Measured n_2 values were combined with n and k data at the same wavelength and evaluated in a simple Kerr phase-shifter. That calculation is asking how much intensity do you need to get a pi phase shift when device length and transmission are competing.

The analysis was guided by three questions. Which solids have a strong Kerr response with limited modeled linear loss? What combinations of material, wavelength band, and length satisfy practical limits for screening? Finally, do the top choices stand up to changes in source variation and objective weight?

The main contribution is a traceable route from published measurements to a short list for experiments. The amount and consistency of supporting evidence is reported next to the modeled performance. Hence, the ranking is a starting point for laboratory work and does not replace nonlinear absorption or optical damage tests.

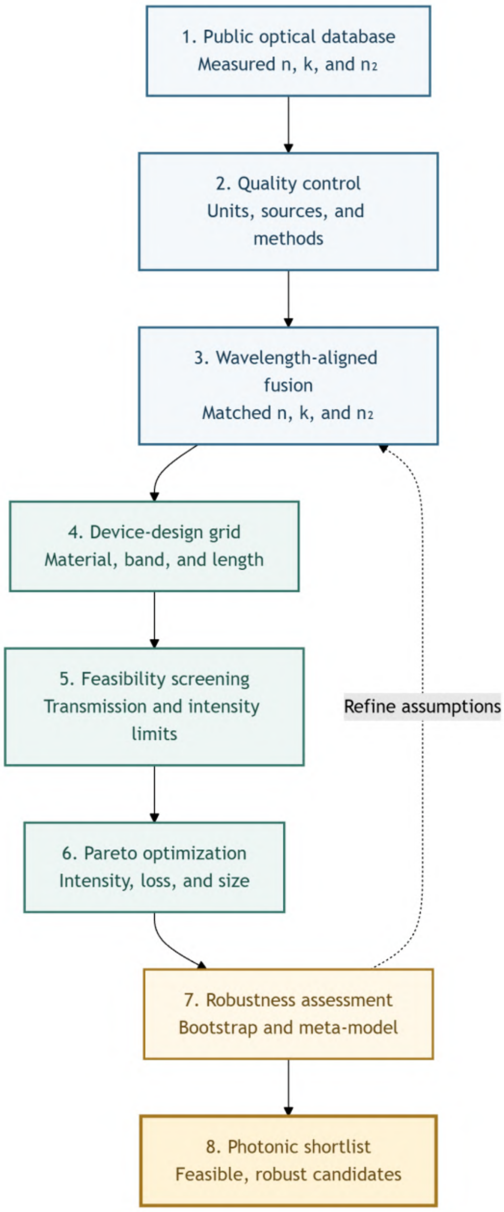

Figure 1. Reproducible workflow for optical-data integration, modeling, and multi-objective screening.

LITERATURE REVIEW AND THEORETICAL FOUNDATION

Intensity-dependent optical response

A third-order polarization response is self-phase modulation, cross-phase modulation, and four-wave mixing. The Kerr contribution of bound electrons lags the applied field by a negligible delay. The scalar relation used here is shown below.

$$n(I) = n_0 + n_2 I \qquad (1)$$

Here, n_0 is the low-intensity refractive index, and n_2 is in m^2 W^{-1}. Using the normal sign convention, n_2 corresponds to self-focusing and n_2, to self-defocusing. Phase control can be supported by both signs if the device is designed for the corresponding phase direction.

The non-linear phase grows with the optical intensity and interaction length. Thus stronger n2 can make device size smaller or drive intensity lower. This relationship gives promise to semiconductors. Their electronic structure can yield a large third-order response at suitable photon energies [13].

Resonance enhancement can further reduce the operating power. Yoshiki and Tanabe [18] demonstrated Kerr switching inside a high Q silica toroid. In addition, silicon waveguides have demonstrated cross-phase switching over millimeter length [2]. Lee et al. realized ultrafast modulation close to 1.5 μm with sub-picosecond pumping [8].

These device demonstrations are not directly translatable to a material ranking. Resonators enhance their field strength at the cost of bandwidth, while waveguides introduce confinement and dispersion. Moreover a bulk coefficient is not equal to an effective waveguide coefficient. We start with intrinsic material data and postpone the device-specific enhancement.

Measurement diversity and comparability

In Z-scan experiments the sample is moved through the focus of a laser beam and the far field transmission is recorded. The resulting trace is used to infer the refraction and absorption. The most common single-beam arrangement was set up by Sheik-Bahae et al. [14]. It has the advantage of a compact apparatus, but still needs accurate characterization of the beam and pulses.

Wave mixing and self-phase modulation have also been used to measure nonlinear refraction. Jansonas et al. [7] used interferometry from near- to mid-infrared, also measuring the spatial and temporal pulse profiles. On the other hand, Flom et al. [6] carried out ultrafast Z-scan measurements at 772, 1030 and 1550 nm.

One reason for different values that are published is pulse length. Longer excitations can allow heating, carrier motion or molecular reorientation to contribute, while short pulses emphasize the electronic response and can open up multiphoton channels. This pulse dependence was observed by Matteo et al. [10] in the nonlinear absorption of long-wave infrared semiconductors.

The crystal direction is another source of dispersion. Directional values for several optical crystals have been reported by Adair et al. [1]. Silicon orientation also changes reported measurements. Tatsuura et al. have also reported different values for silicon crystal directions near 1550 nm. Any summary at the material level must preserve this variation [15].

Optical loss and usable nonlinear phase

The extinction coefficient k describes linear attenuation. Its absorption coefficient obeys a wavelength dependent relation.

$$\alpha = \frac{4\pi k}{\lambda} \qquad (2)$$

The linear intensity transmission through length L is then expressed below.

$$T = \exp(-\alpha L) \, (3)$$

Loss shortens the effective interaction length. This reduces the nonlinear phase gained by the propagating laser. The standard effective length is given next.

$$L_{eff} = \frac{[1 - \exp(-\alpha L)]}{\alpha} \qquad (4)$$

The lossless limit gives Leff equal to L. The nonlinear phase follows from n_2, intensity, wavelength, and effective length.

$$\varphi_{\mathrm{nl}} = \left(\frac{2\pi}{\lambda}\right) n_2 I L_{eff} \quad (5)$$

Setting the phase magnitude to pi gives the required intensity.

$$I_\pi = \frac{\lambda}{(2\mathrm{n}_2 L_{eff})} \quad (6)$$

Equations 2-6 describe an equivalent bulk phase segment, ignoring modal area and optical confinement. Such a simplification allows for a consistent first comparison between materials. The basic concepts of propagation and transfer are well established in stratified optical theory [17].

Research gap

A large amount of nonlinear measurements has been published, but it is still difficult to compare them at the application level. A table of n_2 values does not tell us if useful phase accumulation survives linear loss. Interaction length, number of pieces of evidence and uncertainty have to be taken into account together.

This is, of course, a multi-objective problem: one cannot expect a single design to achieve the minimization of drive intensity, loss and length. In Pareto screening a candidate is kept if no alternative is better in all objectives. This principle is similar to the one used in established evolutionary optimization methods [4].

Since the candidate set is a finite grid of measured material choices, we did an exact non-dominated sorting, rather than a stochastic search. Random weights enter only the later sensitivity analysis. Consequently, the principal frontier does not depend on a chosen weighting scheme.

MATERIALS AND METHODS

Study design and data source

This is a secondary analysis and does not include new laboratory measurements. All the optical data are taken from RefractiveIndex.INFO, where the entries are based on peer-reviewed experiments and other traceable technical references [12].

To ensure reproducibility of the dataset we locked the repository on commit ff11b5897ef0754b15d939d921eb6c745693cbd1 (June 14, 2026). This prevents subsequent revisions of the database from silently changing the results. The same commit will be logged in the companion notebook as well.

All nonlinear files with tabulated n_2 data were read. For each row we kept the material, wavelength, coefficient sign, source file, reference, method and pulse duration. Wavelengths are expressed in μm and n_2 in $m^2 W^{-1}$.

Gas measurements and liquid carbon disulfide were helpful for descriptive plots but were not included in the primary solid-material screen. We didn’t throw away a material just because its n_2 value looked bad. The only data removed was for zeros or invalid entries prior to the logarithm calculations.

Table 1. Dataset scope and analytical design

Field	Value
Public data source	RefractiveIndex.INFO optical constants database
Fixed repository revision	ff11b5897ef0754b15d939d921eb6c745693cbd1
Nonlinear observations	366 valid n_2 points
Materials and records	96 materials; 240 source files
Solid observations	306
Common-band observations	241
Matched n and k observations	169
Material-band summaries	107 total; 66 loss-aware
Device design grid	5346 evaluated combinations
Primary feasible set	820 designs; 23 pairs
Non-dominated set	75 Pareto designs

Data cleaning and source control

The 240 nonlinear source files were not all of the same structure. Some reported a series of wavelengths, so each reported wavelength was a separate observation. When a source listed several pulse durations, they were matched to measurements by position.

Measurement labels were consolidated into Z-scan, self-phase modulation, interferometric, wave-mixing, and other methods. Three entries were not reported without a method label. This broader coding avoided unstable, sparsely populated categories in the meta-regression.

Where available, source tracing DOIs were retained. We did not consider different wavelengths from the same paper as independent studies. We summarized each material-band combination for each source, and then calculated medians of sources.

The selected laser bands were 532, 800, 1030, 1064, 1550, 2000, 3900 and 10600 nm. If the relative distance of a band was not greater than 8%, a measurement was assigned to it. This window accepts nearby experimental wavelengths without wide extrapolation.

Matching linear optical constants

Each nonlinear observation was compared with linear records of the same material at the measured wavelength. We deliberately used the observed wavelength rather than the nominal band center of a laser.

Linear data can be n tables, k tables, combined *n* & *k* tables and one of nine dispersion formula. A formula was evaluated only in the wavelength range provided by its source. Tabulated values were linearly interpolated inside their measured range; no extrapolation was permitted.

At times there were multiple linear records that covered the same material and wavelength. For those cases, the median *n* and *k* dependence on a specific film, orientation or paper decreased. We also kept the number and distribution of contributing records.

A nonlinear record was written to the loss-aware tier only when both n and k were matched. Descriptive summaries kept records with *n* but without *k*, which were excluded from device optimization. The reported zero values of *k* were preserved; they do not imply that absorption is physically absent but that the source did not resolve any loss at the stated precision.

Laser phase-shifter model

The model of the phase-shifter is a uniform region of optical interaction. We tested 81 logarithmically spaced lengths from 10 μm to 10 mm. For each pair of material-band the median values of n$_2$, n$_0$ and k at the source level were estimated.

Equations 2–6 gave the absorption coefficient, transmission, effective length, and intensity required for a pi phase shift. Insertion loss was followed by transmission loss and relative index perturbation was calculated as $\Delta n/n_0$.

A design was considered possible when the linear transmission was 90%, the pi-shift intensity was less than 100 GW cm-2^{-2} and Delta($\Delta n/$n)/n0$_0$ was less than 1%. These limits are engineering comparison filters and are not to be read as damage or safety thresholds.

The model ignores nonlinear absorption, optical damage or modal confinement. This limitation was accepted because of the lack of a consistent beta data set across the material set. Thus the comparison below is only between Kerr efficiencies under constraints of linear loss.

Multi-objective selection

We evaluate the finite grid directly without fitting a surrogate. The three quantities to be minimized were the pi-shift intensity, insertion loss and interaction length. A design was non-dominated if there was no other design that was better than the design in all three quantities at the same time.

We also selected a representative balanced design for each possible material-band combination. Intensity, loss and length were normalized to [0,1] range within that pair. The selected point was the one with the smallest Euclidean distance to the local ideal.

An independent equal-weight score also summarized phase efficiency, transmission, compactness, evidence count and repeatability for presentation. It was not used to build the Pareto set, which remained the main optimization result.

We tested ranking sensitivity using 3,000 weight vectors drawn from a Dirichlet distribution. When the draw was made the weighting of the five score components changed. Then we noted how many times each candidate appeared in the top five or top ten.

Statistical analysis

The uncertainty of the leading material-band pairs was estimated with 4,000 source-level bootstrap samples. Resampling was done within pairs. Pairs that had a single source necessarily produced degenerate intervals, and so were flagged because the between-study variation could not be estimated.

$\log_{10}|n_2|$ was used as the outcome in the meta-regression. The predictors were log wavelength, log pulse duration, material family and method group and continuous terms were standardized. Chalcogenides served as the material reference and interferometry as the method reference.

This model included 301 solid-material measurements with reported pulse durations. Confidence intervals came from 800 clustered bootstrap draws that resampled 83 materials. For five-fold grouped cross-validation, whole materials (instead of rows) were held-out.

Sensitivity checks varied minimum transmission across 80%, 90%, and 95% and applied intensity caps of 10, 100, and 1000 GW cm^{-2}. The nine combinations show whether the shortlist is an artifact of one chosen threshold.

Integrity of repetition and search

All processing was performed in Python with random seed 42. The companion Colab notebook states each cleaning rule, recreates the tables and figures, and exports both cleaned observations and a machine-readable result.

RESULTS

Dataset coverage

The non-linear data set was cleaned and included 366 measurements from 240 source files and 96 materials. Of these measurements, 306 were of solids and 241 were near one of the selected laser bands.

Most frequently measured was silicon. The coverage for silica, ZnSe, ZnS, nitrogen, and magnesium fluoride was relatively broad but unevenly distributed. The majority of the observations were made near 1 μm and few infrared laser lines were found.

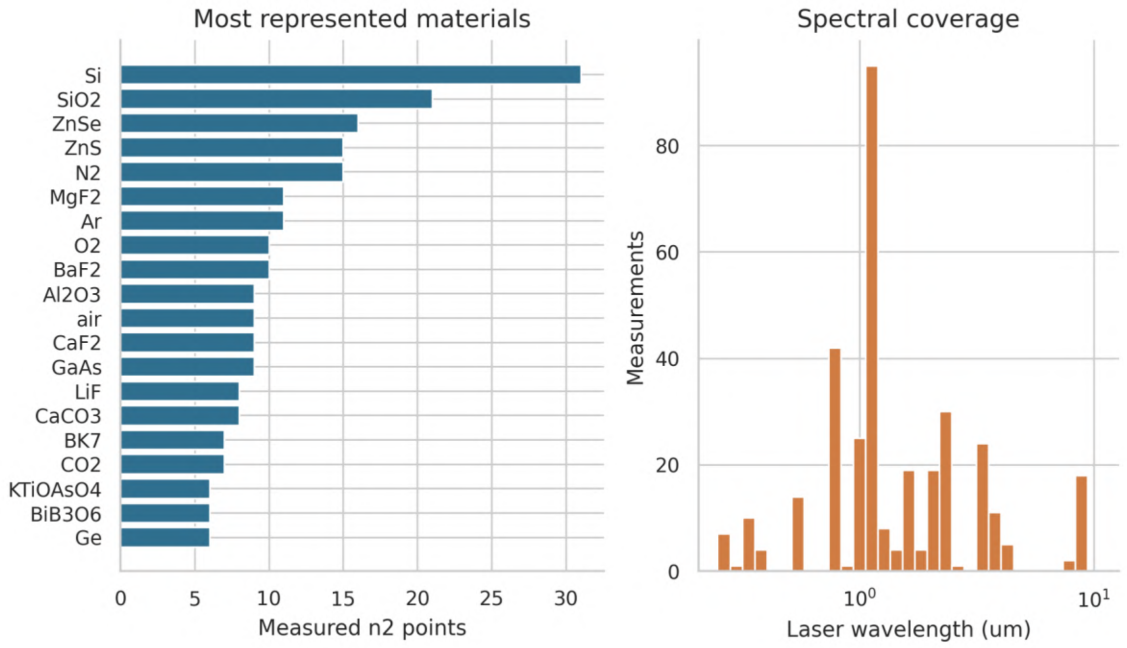

Figure 2. Material and wavelength coverage in the nonlinear dataset.

Measured n_2 spans more than ten orders of magnitude. Semiconductors and some crystals were on the high side, gas values were on the low side. It is just as important that there is a substantial overlap between families and that this argues against ranking by family name alone.

The distribution shows that the information in the material family is useful but not predictive of the response. Wavelength and experimental conditions can account for part of the remaining spread.

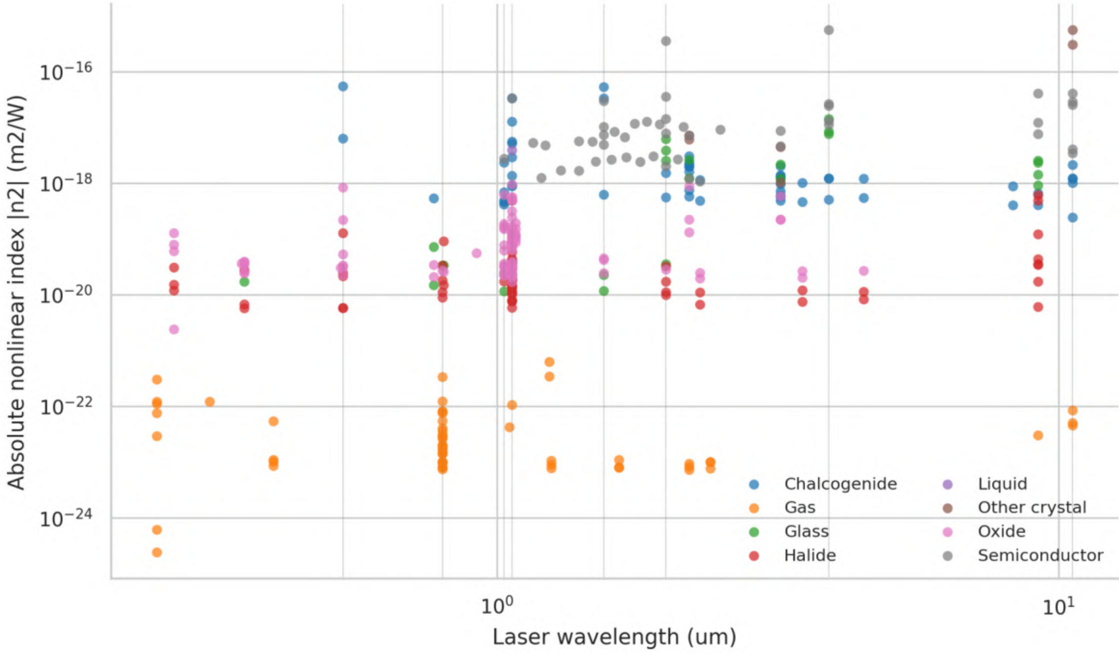

Figure 3. Measured absolute Kerr coefficients across wavelength and material family.

Both *n* and *k* could be matched for 169 nonlinear measurements. Collapsing repeated observations within sources produced 107 solid material-band pairs, of which 66 had sufficient loss information for device modeling.

Material Performance Related to Loss Consciousness

The loss-aware map could disentangle a strong Kerr coefficient from a useful low-loss response. Some of the semiconductor measurements gave high phase metrics and low tabulated k-values. Oxides and halides generally showed lower modeled phase efficiency, though their damage tolerance was outside of the scope of this comparison.

GaAs was observed at some of the most intense modeled positions, and CdS demonstrated a strong response at around 1064 nm. Silicon was not so extreme, but had several measurements to support. ZnSe did not have such high peak efficiency, but covered larger number of laser bands.

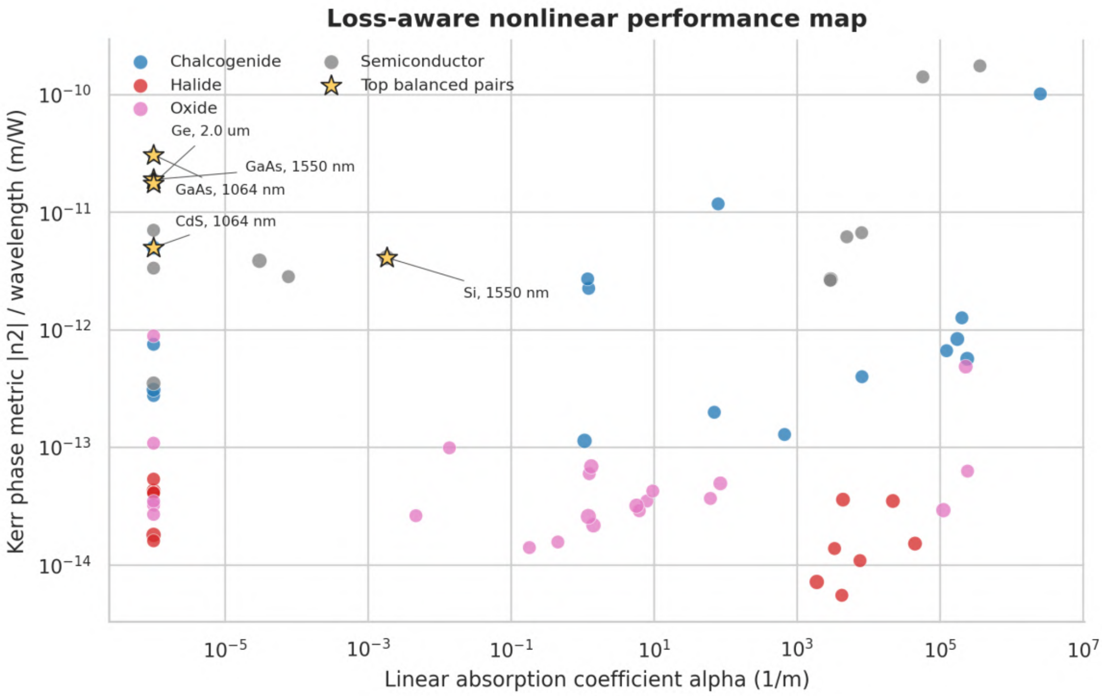

Figure 4. Kerr phase metric against wavelength-matched linear absorption. Starred points mark the five leading balanced pairs.

Feasible designs and Pareto frontier

Of the 5,346 modeled combinations, 820 satisfied all three screening constraints. They came from 23 material-band pairs. Exact sorting placed 75 of the feasible designs on the non-dominated frontier.

Under the balanced score, GaAs at 1064 nm occupied first place. Its median $|n_2|$ was 3.26×10^{-17} m² W⁻¹. At the representative length of 0.410 mm, the model required 3.98 GW cm⁻² for a pi phase shift.

CdS at 1064 nm was the second-ranked pair, based on a median $|n_2|$ of 5.30×10^{-18} m² W⁻¹. Its representative design required 10.33 GW cm⁻² across 0.972 mm. The median was supported by two orientation-dependent measurements [1].

The next positions were GaAs at 1550 nm, Ge at 2.0 µm, and silicon at 1550 nm. The silicon result drew on four source records and required 12.56 GW cm⁻² over 0.972 mm.

Of the 5,346 modeled combinations, 820 met all three screening constraints. They were assembled from 23 pairs of material-bands. Exact sorting identified 75 of the feasible designs on the nondominated frontier.

GaAs at 1064 nm was ranked first in the balanced score. Its median $|n_2|$ was 3.26×10^{-17} m² W⁻¹. The model required 3.98 GW cm⁻² for a pi phase shift at the representative length of 0.410 mm.

CdS at 1064 nm was the second-ranked pair, based on a median $|n_2|$ of 5.30×10^{-18} m² W⁻¹. The representative design required 10.33 GW cm⁻² over 0.972 mm. The median was sustained by two orientation-dependent measurements [1].

Next positions were GaAs at 1550 nm, Ge at 2.0 µm and silicon at 1550 nm. The silicon result was based on four source records and required 12.56 GW cm-2 over 0.972 mm.

Table 2. Ten leading balanced material-band designs

Rank	Material / band	Median n_2 (m^2W^{-1})	Sources	I-pi (GW cm^{-2})	Length (mm)	T(%)	Score
1	GaAs 1064 nm	3.26×10^{-17}	1	3.98	0.410	100.000	0.764
2	CdS 1064 nm	5.30×10^{-18}	2	10.33	0.972	100.000	0.738
3	GaAs 1550 nm	2.93×10^{-17}	1	4.98	0.531	100.000	0.737
4	Ge 2.0 µm	3.50×10^{-17}	1	5.38	0.531	100.000	0.732
5	Si 1550 nm	6.35×10^{-18}	4	12.56	0.972	100.000	0.694
6	GaAs 2.0 µm	1.40×10^{-17}	1	8.01	0.891	100.000	0.680
7	GaAs 3.9 µm	1.30×10^{-17}	1	11.91	1.259	100.000	0.637
8	Si 3.9 µm	1.10×10^{-17}	1	14.08	1.259	100.000	0.627
9	ZnSe 1064 µm	2.87×10^{-18}	1	14.74	1.259	99.851	0.605
10	Si 2.0 µm	7.70×10^{-18}	3	12.26	1.059	100.000	0.596

Here T is approximated by linear transmission. If the source-level median of k is reported as zero, the model can return T = 100%.

Across the leading pairs, increasing interaction length lowered the required intensity. Absorption eventually reduced that benefit for lossy materials. At short lengths, the 100 GW cm^{-2} constraint removed candidates with weaker nonlinear response.

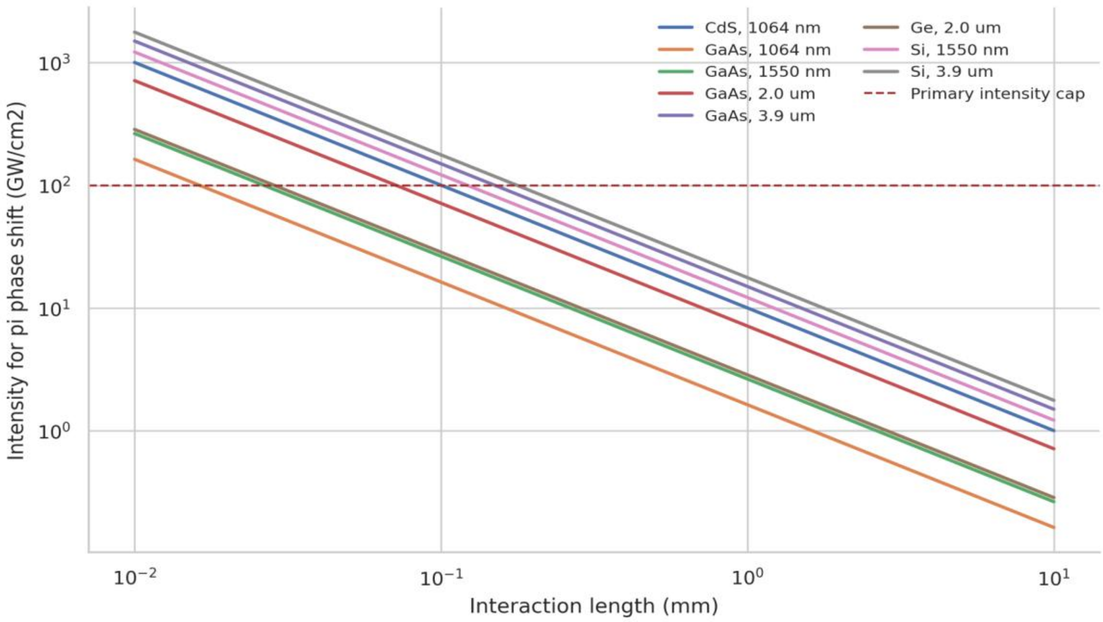

Figure 5. Modeled length-intensity trade-offs for leading material-band pairs

Many frontier points had very small modeled loss, including several with a reported median k of zero. A small floor was introduced only to display those points on a logarithmic axis. That plotting floor was used by neither feasibility nor numerical rank.

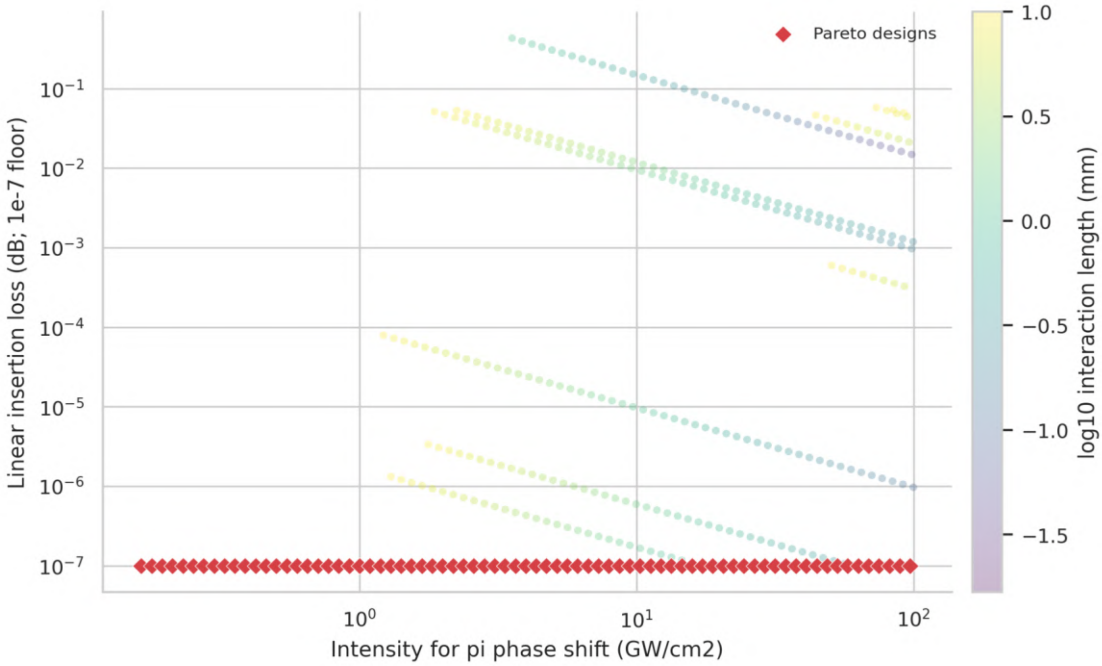

Figure 6. Feasible design space and non-dominated frontier. The visual loss floor equals $\mathbf{10^{-7}}$ dB.

Performance near common laser bands

The band-by-band heatmap showed the materials perform very spectrally. For example, GaSb was reported to have exceptionally large values in several infrared bands, but was not loss-aware meeting the requirements for the main shortlist.

GaAs remained competitive from 1064 nm to 3.9 μm, then weakened near 10.6 μm. Ge was strongest in the mid-infrared. Silicon gave smaller coefficients, but better evidence at ~1550 and ~2000 nm.

ZnSe exhibited a moderate response in a relatively broad spectral range. Two independent studies agreed closely near 3.9 μm [5,16]. Three sources with different pulse durations had median n_2 of 1.20×10^{-18} m^2 W^{-1} [10, 11].

Source uncertainty and ranking stability

The apparent leaders did not have equal evidential support. The accepted GaAs estimate at 1064 nm came from one nonlinear source, making between-study variation impossible to calculate. The same limitation was observed in the GaAs result at 1550 nm and the Ge result at 2.0 μm.

In silicon, 4 sources are supported at 1550 nm with a median n2 of 6.35 x 10-18 m2/W. Its bootstrap interval was wider than intervals for one-source pairs, reflecting real disagreement among published measurements [3, 9, 15].

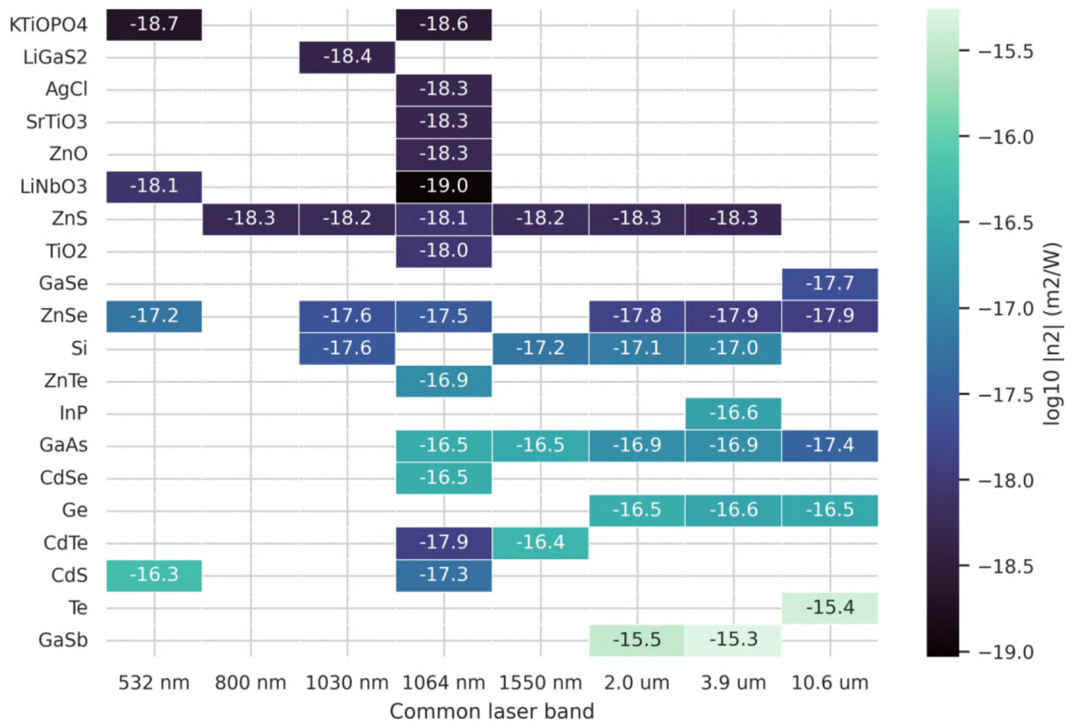

Figure 7. Median nonlinear response near eight common laser bands. Blank cells lack a nearby accepted measurement.

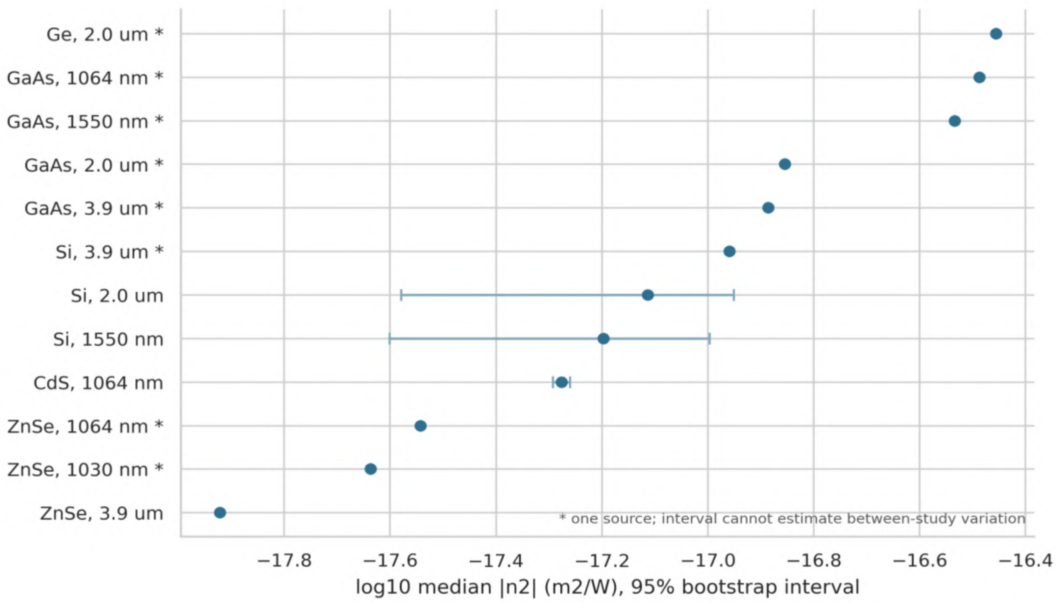

Figure 8. Source-level bootstrap intervals for leading material-band pairs. Asterisks mark one-source estimates.

The analysis with random weights also had the same group at the top but in a different order. GaAs at 1064 nm was among the top five 87.8% of the time, as compared to 88.6% for CdS at 1064 nm. The respective probabilities were 83.8% for GaAs at 1550 nm and 71.3% for Ge at 2.0 µm.

Silicon at 1550 nm was in the top five in 46.6% of draws and had a median rank of six. Its chance of a top ten was 69.8 per cent. This follows a typical trade-off pattern where silicon has more extensive evidence but lower raw Kerr efficiency than the top pairs.

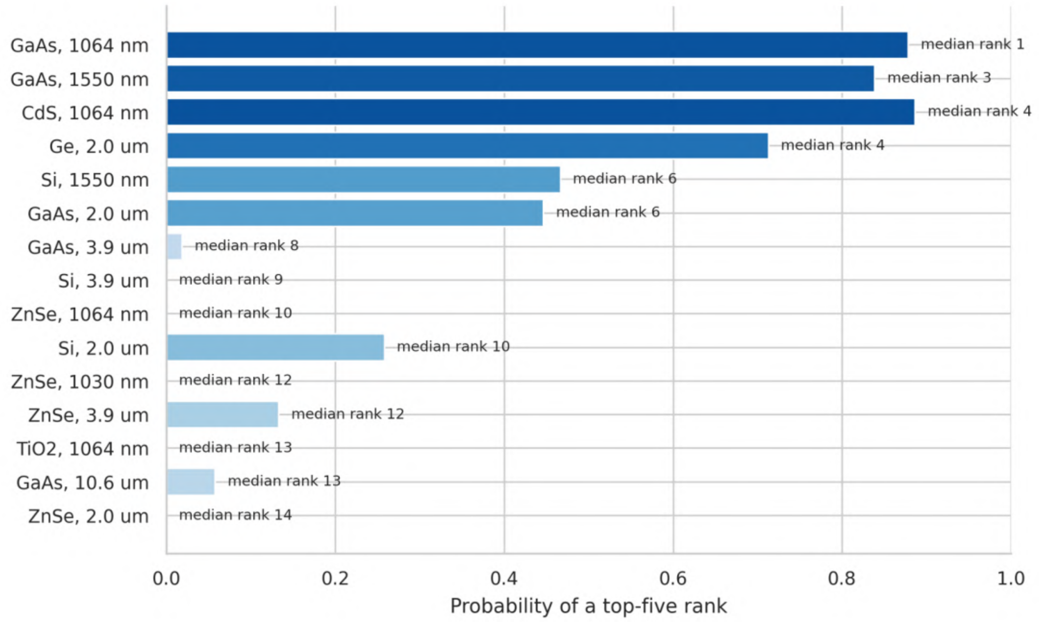

Figure 9. Ranking stability across 3,000 random objective-weight vectors

Meta-regression and sensitivity

The meta-regression was based on 301 observations on 83 solid materials. It accounted for 74.7% of the variance in the sample, and grouped cross-validation resulted in a mean R^2 of 0.534 with a fold standard deviation of 0.148.

The semiconductor coefficient was 0.757 relative to chalcogenides. The 95% clustered interval was from 0.221 to 1.903. Halides had a coefficient of −1.691. Oxides showed -1.159. Both intervals remained negative.

Wavelength had a coefficient of 0.201. Pulse duration coefficient was 0.149. Both ranges include zero. The coefficients for method-groups also included zero. These are correlational, not causal estimates.

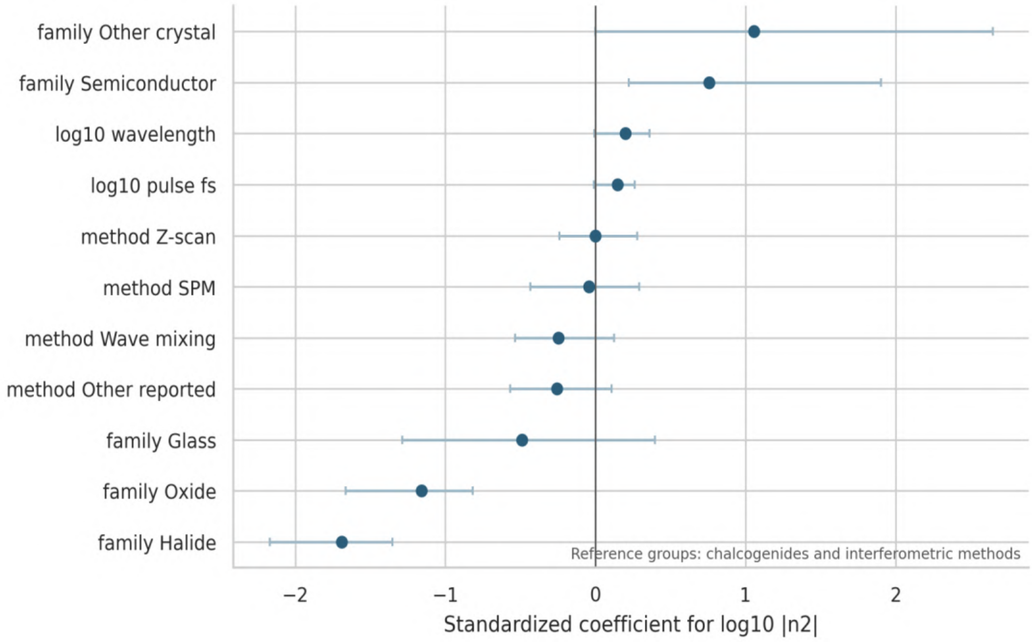

Figure 10. Cluster-bootstrap coefficients for log10 absolute n_2. Continuous predictors were standardized.

Depending on the thresholds, between 14 and 44 material-band pairs remained feasible. The strict limit of 10 GW cm^{-2} kept 14 pairs at each transmission level, whereas the limit of 1000 GW cm^{-2} kept 41-44 pairs.

In all cases GaAs at 1064 nm remained the leading low-cost candidate. This is relative to the current model only. It does not address nonlinear absorption or damage.

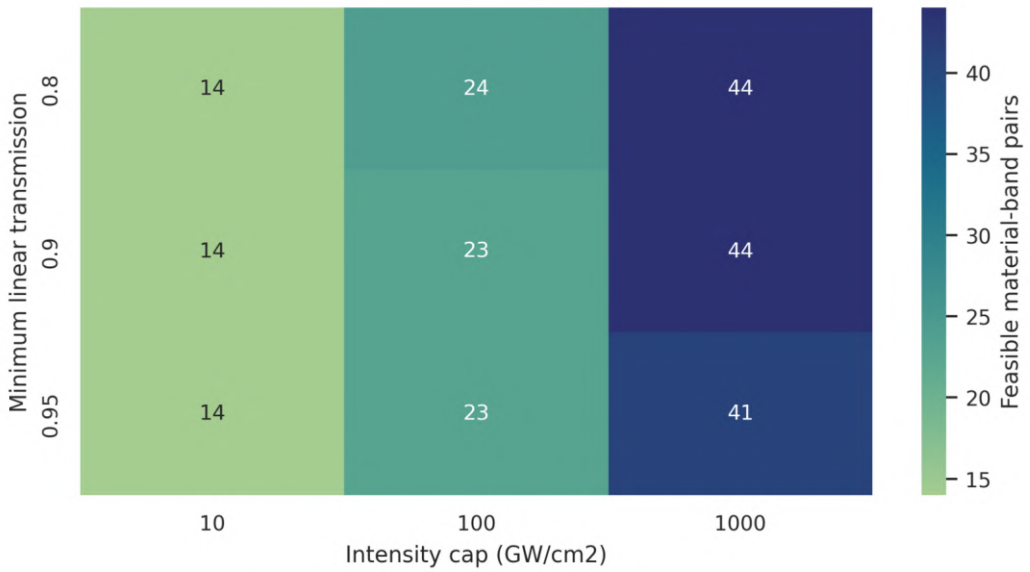

Figure 11. Feasible material-band counts under changed transmission and intensity limits.

DISCUSSION

Meaning of the leading candidates

For the present model, the best phase response is obtained for GaAs at 1064 nm. This result is physically plausible since large bound-electronic nonlinearities can occur near semiconductor transitions [13]. Here, the measured coefficient translates into a short calculated interaction region rather than a direct claim about device power.

Several details temper this first-place result. The accepted GaAs value came from one experiment using 40 ps pulses, so its reproducibility and transfer to femtosecond excitation are unknown. Likewise, a median k reported as zero describes the resolution of the linear source; it is not proof of perfect transparency.

GaAs also performed strongly near 1550 nm, but this estimate is again supported by a narrow evidence base. The accepted value came from Tatsuura et al. [15], whose main focus was switching in CdTe and whose broader measurements included semiconductor crystals. A practical GaAs design therefore needs a matched set of linear and nonlinear measurements.

CdS at 1064 nm is supported by two directional values, giving more information about orientation than the leading GaAs pair. Both measurements, however, used 3 ns pulses. Slow processes may have contributed, so the estimate should not be carried unchanged into a femtosecond design.

The large negative n_2 reported for Ge at 2.0 μm reduced the modeled phase-shift intensity. Its sign reverses the phase direction rather than eliminating the effect, which may be accommodated through circuit bias. Strong wavelength dependence in infrared materials has also been reported by Ensley and Bambha [5].

Silicon at 1550 nm has the most developed evidence among the five leading pairs. Four source records contributed to its median, which is consistent with established nonlinear measurements [3, 9]. Independent switching experiments further show that this response can produce useful phase modulation in silicon waveguides [2, 8].

But that maturity doesn't address silicon's main weakness. Beta is missing from our screen. Two-photon absorption is large near 1550 nm. Hence the calculated phase efficiency is optimistic for silicon and probably for other semiconductors; a device level comparison must include nonlinear loss.

ZnSe did not achieve the peak semiconductor scores, but it did provide coverage from the near-infrared to the long-wave infrared. Two sources agreed near 3.9 μm and three pulse regimes were characterized at 10.6 μm. The broad spectral range of ZnSe makes it a useful reference material for the proposed infrared validation.

The present ranking is pushed down by lower n_2 values of oxides and halides. This is not to be taken as poor suitability for high power optics. These materials are often favored for their low nonlinear absorption and high damage thresholds, but neither of these properties is included here. Thus a damage-aware objective set can have a significant impact on their position.

Methodological value

The process introduces four useful capabilities to a standard coefficient table: source traceability, loss matching at the same wavelength, a weight independent Pareto frontier and an explicit representation of evidence gaps. These features together show why a large reported n_2 is not enough by itself.

This summarization within sources prior to pooling prevents a paper with many nearby wavelength points from dominating the median. This is particularly true for silicon. If each reported wavelength were taken as an independent experiment, it would have an uncertainty narrower than the evidence justifies.

Grouped cross-validation yields a similarly conservative test of the meta-regression. A random row split would allow measurements of one material to leak into both training and test sets. The expected reduction in R^2 was achieved by withholding whole materials.

The equal weight score is useful for showing a short list, but its priorities are not universal. In a high-power laser application, one may prioritize transmission and damage resistance, whereas in an integrated switch, intensity and footprint may be critical. The random-weight experiment measures how much those choices shuffle candidates.

Comparison with practical photonic systems

The calculated interaction lengths are compatible with the scales involved in bulk and integrated photonics. Millimeter-scale silicon waveguides have already supported switching: Boyraz et al. [2] used an interferometric arrangement, and Lee et al. [8] reported a 5 mm device driven with low pulse energy.

A resonator can amplify the field within the cavity, reducing the necessary power from the outside. This effect was demonstrated by Yoshiki and Tanabe [18] in a low power silica Kerr switch. Our bulk-equivalent calculation is purposely not enhanced this way.

Thus, a direct comparison with the reported power of the device would be misleading. Internally we have intensity in the material. Measured device power is a function of mode area, coupling, quality factor, and pulse shape. The idea of the shortlist is to lead, not substitute the following device simulation.

Experimental validation plan

A useful validation campaign would begin with GaAs and CdS at 1064 nm, followed by GaAs at 1550 nm, Ge at 2.0 µm, and silicon at 1550 nm. ZnSe at 3.9 µm should be added as an infrared reference because its evidence is broader than its rank suggests.

Table 3. Proposed matched-sample validation matrix

Candidate	Reason for selection	Required validation
GaAs, 1064 nm	Highest modeled efficiency; one n_2 source	Repeat n_2 across pulse lengths; measure nonlinear absorption and damage
CdS, 1064 nm	Two directional values; nanosecond evidence	Repeat with femtosecond pulses; test anisotropy and thermal response
GaAs, 1550 nm	High modeled response; one n2 source	Measure n_2, two-photon absorption, carriers, and damage on one sample
Ge, 2.0 µm	Large negative n_2; one source	Confirm sign; measure multiphoton absorption and free carriers
Si, 1550 nm	Four sources and mature device platform	Measure two-photon loss, carrier lifetime, and waveguide effective area
ZnSe, 3.9 µm	Two agreeing infrared sources	Measure nonlinear absorption onset and damage under application pulses

The linear and nonlinear properties should be measured on the same specimen. Spectroscopic ellipsometry can give n and k, then Z-scan or interferometry can give n2 and nonlinear absorption. The pulse duration should be suitable for the application.

Damage testing should use the same wavelength, pulse width, repetition rate, and spot size as the nonlinear measurement. Separate measurement to detect thermal accumulation. For such semiconductors also the generation and relaxation of the carriers should be resolved.

A second stage should then embed the measured properties into a given waveguide or resonator model. Mode overlap, effective area, dispersion, and interfaces then enter the phase calculation. A robust choice of device can only be made after including the fabrication tolerances.

LIMITATIONS

There are several limitations to the interpretation of the rankings. The secondary measurements were made in different laboratories, and were not consistent in calibration, sample purity, temperature or orientation. Median aggregation limits the influence of outliers but does not correct a systematic difference between experiments.

In many cases n and k were derived from something other than the nonlinear measurement. Hence the records may refer to different specimens, phases or preparation histories. Matching wavelength makes the comparison better, but does not guarantee the equivalence of samples.

A tabulated k of zero usually means that absorption was not resolved at the source's precision. Therefore a calculated transmission of 100 % should not be interpreted as an indication of a perfectly transparent sample.

The phase model includes linear loss only. Two- and three-photon absorption, free-carrier effects and heating were omitted although they can dominate strong-field operation. One example of this limitation is the pulse-dependent absorption reported by Matteo et al. [10] for infrared semiconductors.

The model also considers intensity as a bulk quantity. There is no modal confinement, effective area, or resonant buildup, so the reported intensity alone does not permit recovery of device power . There are also no coupling and scattering losses.

An alternative analytical choice is the assignment of measurements within 8% of a nominal laser band. It does not extrapolate to long ranges, but may still group points over a narrow resonance. The exported observation table may be used with a tighter window by future users.

Finally, the evidence is spotty. Several major pairs are described by a single nonlinear source, so bootstrap intervals for them contain no information about replication across studies. Such candidates should be considered tentative until independent measurements are obtained.

CONCLUSION

This analysis compares 366 observations on a common phase shifter basis for 96 materials, combining measured Kerr coefficients with wavelength matched linear constants.

The engineering screen retained 820 designs from 23 material-band pairs, with 75 designs on the Pareto frontier. The best balanced score was obtained with GaAs at 1064 nm followed by CdS at the same wavelength.

Silicon at 1550 nm had lower modeled efficiency, but much better source support. The final selection among these materials must take into account nonlinear absorption, optical damage and measurements on matched samples. The accompanying Colab workflow provides a reproducible basis for that extension.

Data and Code Availability

The underlying data are available through RefractiveIndex.INFO. The database description is published at https://doi.org/10.1038/s41597-023-02898-2. The repository is available at https://github.com/polyanskiy/refractiveindex.info-database. The attached notebook fixes the commit and reproduces all outputs shown in the report. The figures in this paper are derived from the data analyzed in this paper.

REFERENCES

1. Adair, R., Chase, L. L., & Payne, S. A. (1989). Nonlinear refractive index of optical crystals. *Physical Review B, 39*, 3337-3350. https://doi.org/10.1103/PhysRevB.39.3337
2. Boyraz, O., Koonath, P., Raghunathan, V., & Jalali, B. (2004). All optical switching and continuum generation in silicon waveguides. *Optics Express, 12*, 4094-4102. https://doi.org/10.1364/OPEX.12.004094
3. Bristow, A. D., Rotenberg, N., & van Driel, H. M. (2007). Two-photon absorption and Kerr coefficients of silicon for 850-2200 nm. *Applied Physics Letters, 90*, 191104. https://doi.org/10.1063/1.2737359
4. Deb, K., Pratap, A., Agarwal, S., & Meyarivan, T. (2002). A fast and elitist multiobjective genetic algorithm: NSGA-II. *IEEE Transactions on Evolutionary Computation, 6*, 182-197. https://doi.org/10.1109/4235.996017
5. Ensley, T. R., & Bambha, N. K. (2019). Ultrafast nonlinear refraction measurements of infrared transmitting materials in the mid-wave infrared. *Optics Express, 27*, 37940-37951. https://doi.org/10.1364/OE.380702
6. Flom, S. R., Beadie, G., Bayya, S. S., Shaw, B., & Auxier, J. M. (2015). Ultrafast Z-scan measurements of nonlinear optical constants of window materials. *Applied Optics, 54*, F123-F130. https://doi.org/10.1364/AO.54.00F123
7. Jansonas, G., Budriunas, R., Vengris, M., & Varanavicius, A. (2022). Interferometric measurements of nonlinear refractive index in the infrared spectral range. *Optics Express, 30*, 30507-30524. https://doi.org/10.1364/OE.458850
8. Lee, J. Y., Yin, L., Agrawal, G. P., & Fauchet, P. M. (2010). Ultrafast optical switching based on nonlinear polarization rotation in silicon waveguides. *Optics Express, 18*, 11514-11523. https://doi.org/10.1364/OE.18.011514
9. Lin, Q., Zhang, J., Piredda, G., Boyd, R. W., Fauchet, P. M., & Agrawal, G. P. (2007). Dispersion of silicon nonlinearities in the near infrared region. *Applied Physics Letters, 91*, 021111. https://doi.org/10.1063/1.2750523
10. Matteo, D., Tochitsky, S., Pigeon, J., & Joshi, C. (2024). Pulse length effects in the nonresonant long-wave infrared nonlinear optical response of n-Ge, GaAs, and ZnSe. *Journal of the Optical Society of America B, 41*, E35-E44. https://doi.org/10.1364/JOSAB.534031
11. Pigeon, J. J., Matteo, D. A., Tochitsky, S. Y., Ben-Zvi, I., & Joshi, C. (2020). Measurements of the nonlinear refractive index of AgGaSe2, GaSe, and ZnSe at 10 µm. Journal of the Optical Society of America B, 37, 2076-2082. https://doi.org/10.1364/JOSAB.395844
12. Polyanskiy, M. N. (2024). Refractiveindex.info database of optical constants. *Scientific Data, 11*, 94. https://doi.org/10.1038/s41597-023-02898-2

13. Sheik-Bahae, M., Hutchings, D. C., Hagan, D. J., & Van Stryland, E. W. (1991). Dispersion of bound electron nonlinear refraction in solids. *IEEE Journal of Quantum Electronics*, *27*, 1296-1309. https://doi.org/10.1109/3.89946
14. Sheik-Bahae, M., Said, A. A., Wei, T. H., Hagan, D. J., & Van Stryland, E. W. (1990). Sensitive measurement of optical nonlinearities using a single beam. *IEEE Journal of Quantum Electronics*, *26*, 760-769. https://doi.org/10.1109/3.53394
15. Tatsuura, S., Matsubara, T., Mitsu, H., Sato, Y., Iwasa, I., Tian, M., & Furuki, M. (2005). Cadmium telluride bulk crystal as an ultrafast nonlinear optical switch. *Applied Physics Letters*, *87*, 251110. https://doi.org/10.1063/1.2151256
16. Werner, K., Hastings, M. G., Schweinsberg, A., Wilmer, B. L., Austin, D., Wolfe, C. M., Kolesik, M., Ensley, T. R., Vanderhoef, L., Valenzuela, A., & Chowdhury, E. (2019). Ultrafast mid-infrared high harmonic and supercontinuum generation with n2 characterization in zinc selenide. *Optics Express*, *27*, 2867-2885. https://doi.org/10.1364/OE.27.002867
17. Yeh, P., Yariv, A., & Hong, C. S. (1977). Electromagnetic propagation in periodic stratified media. I. General theory. *Journal of the Optical Society of America*, *67*, 423-438. https://doi.org/10.1364/JOSA.67.000423
18. Yoshiki, W., & Tanabe, T. (2014). All-optical switching using Kerr effect in a silica toroid microcavity. *Optics Express*, *22*, 24332-24341. https://doi.org/10.1364/OE.22.024332
19. Najeeb Ahmed , O., & Amer Mohammed, A. (2026). Intelligent Deep Learning-based Systems to Detect Early Cyber Attacks in IoT Networks. Libyan Journal of Applied and Contemporary Sciences, 1(1), 38–52. https://doi.org/10.64943/ljacs.2026.010105

تحسين الاستجابة البصرية المستحدثة بالليزر في المواد المتقدمة من أجل تطبيقات فوتونية عالية الأداء

الملخص

تعتمد العديد من المفاتيح الضوئية، والمعدلات، والمستشعرات، وأجهزة التحكم الطيفي على التغيرات الضوئية في معامل الانكسار. ويصعب إيجاد مادة مناسبة، لأن معاملات اللاخطية المنشورة تعتمد على الطول الموجي، ومدة النبضة، وطريقة القياس. وللتغلب على هذه المشكلة، أجرينا تحليلًا يراعي الفقد على بيانات تجريبية متاحة للعموم. تضمنت مجموعة البيانات 366 قياسًا لمعامل الانكسار اللاخطي من 240 سجلًا مصدريًا، وغطت 96 مادة. في جميع الحالات، تم ضبط بيانات معامل الانكسار الخطي وبيانات الانطفاء عند نفس الطول الموجي للقياس اللاخطي. استُخدمت هذه القيم في نموذج مُزحزح طور كير الذي يربط استجابة المادة بالنفاذية، وطول التفاعل، وشدة الإشارة. اختبرنا 5346 تركيبة من المادة وطول النطاق. تطلبت التصاميم القابلة للتنفيذ نفاذية خطية لا تقل عن 90%، وشدة نبضة باي لا تتجاوز 100 جيجا واط/سم²، وتغيرًا في معامل الانكسار أقل من 1%. أسفرت هذه الشروط عن 820 تصميمًا من 23 زوجًا من المواد والنطاقات، بما في ذلك 75 حلًا غير مُهيمن. وُجد التوازن الأمثل لزرنيخيد الغاليوم عند 1064 نانومتر، والذي يُعطي شدة إزاحة باي مُنمذجة تبلغ 3.98 جيجا واط/سم² على مسافة 0.410 مم. مع ذلك، جاء هذا التقدير من مصدر غير خطي واحد. وجاء السيليكون عند 1550 نانومتر في المرتبة الخامسة بأربعة مصادر، بمتوسط معامل غير خطي قدره 6.35×10^{-18} م²/واط. أوضح تحليل الانحدار التجميعي 74.7% من التباين الملحوظ، وأسفر التحقق المتقاطع المُجمّع عن متوسط R^2 قدره 0.534. حتى بعد التصحيح، ظلت قياسات أشباه الموصلات أعلى من مجموعة الكالكوجينيد المرجعية. تُعد القائمة المختصرة المُنشأة مفيدة للفرز، ولكن لا يزال التحقق المباشر من الامتصاص غير الخطي وحدود التلف وحصر الموجة في الدليل الموجي ضروريًا.

الكلمات المفتاحية: معامل انكسار غير خطي؛ تأثير كير ؛ التبديل الضوئي؛ تحسين باريتو؛ بيانات تجريبية ثانوية؛ الفوتونيات القابلة للتكرار.